Shear-induced instabilities in layered liquids

Günter K. Auernhammer* and Helmut R. Brand

Theoretische Physik III, Universität Bayreuth, 95440 Bayreuth, Germany

Harald Pleiner

Max-Planck-Institute for Polymer Research, P.O. Box 3148, 55021 Mainz, Germany

Motivated by the experimentally observed shear-induced destabilization and reorientation of smectic-A-like systems, we consider an extended formulation of smectic-A hydrodynamics. We include both, the smectic layering (via the layer displacement u and the layer normal $\hat{p}$) and the director $\hat{n}$ of the underlying nematic order in our macroscopic hydrodynamic description and allow both directions to differ in nonequilibrium situations. In an homeotropically aligned sample the nematic director does couple to an applied simple shear, whereas the smectic layering stays unchanged. This difference leads to a finite (but usually small) angle between $\hat{n}$ and $\hat{p}$, which we find to be equivalent to an effective dilatation of the layers. This effective dilatation leads, above a certain threshold, to an undulation instability of the layers. We generalize our earlier approach [G. K. Auernhammer, H. R. Brand, and H. Pleiner, Rheol. Acta **39**, 215 (2000)] and include the cross couplings with the velocity field and the order parameters for orientational and positional order and show how the order parameters interact with the undulation instability. We explore the influence of various material parameters on the instability. Comparing our results to recent experiments and molecular dynamic simulations, we find a good qualitative agreement.

I. INTRODUCTION

Submitted to an applied shear flow, many complex liquids show an interesting coupling between their internal structure and the flow field. For smectic-A-like systems (including block copolymers, lyotropic systems, and side-chain liquid crystalline polymers) this coupling may induce reorientation of the layers. Experiments on a variety of systems which differ significantly in their microscopic details show, nevertheless, striking similarities in their macroscopic behavior under shear. The systems under investigation include block copolymers [1–6], low molecular weight (LMW) liquid crystals [7–9], lyotropic lamellar phases (both LMW [10–12] and polymeric [13]), and liquid crystalline side-chain polymers [14,15]. These experiments use either a steady shear (typically for the low-viscosity systems, e.g., in a Couette cell) or large amplitude oscillatory shear (often in the highly viscous polymeric systems, e.g., in a cone-plate or plate-plate geometry). Due to these experimental differences a direct comparison between the different systems is not always straightforward. The common features of all these experiments can be described as follows. Starting with an aligned sample where the layers are parallel to the planes of constant velocity ("parallel" orientation), the layering is stable up to a certain critical shear rate [2,5,8–11,13]. At higher shear rates two different situations are observed. Depending on the system, either multilamellar vesicles [10,12,13] ("onions," typically in lyotropic systems) or layers perpendicular to the vorticity direction [1–5,8,9,14] ("perpendicular" orientation, typically in solvent free sys-

tems) form. In some of the systems a third regime is observed at even higher shear rates with a parallel orientation [5,10]. If the starting point is rather a randomly distributed lamellar phase, the first regime is not observed [1,4,12,16]. This last point illustrates that experiments on layered liquids depend on the history of the sample. In our further discussion we will restrict ourselves to systems showing a well aligned parallel orientation before shear is applied.

The experimental similarities between different systems indicate that the theoretical description of these reorientations can be constructed, at least to some extent, from a common basis independent of the actual system (on the other hand, a description including the differences between the systems under investigation must refer closer to their microscopic details). When looking for a macroscopic description, the well established standard smectic-A hydrodynamics [17–20] is a good starting point for such a theoretical approach.

As first shown by Delaye *et al.* [21] and Clark and Meyer [22], thermotropic smectic-A liquid crystals are very sensitive against dilatations of the layers. Above a very small, but finite, critical dilatation, the liquid crystal develops undulations of the layers to reduce the strain locally. Oswald and Ben-Abraham considered dilated smectic A under shear [23]. When a shear flow is applied (with a parallel orientation of the layers), the onset for undulations is unchanged only if the wave vector of the undulations points in the vorticity direction (a similar situation was later considered in Ref. [24]). Whenever this wave vector has a component in the flow direction, the onset of the undulation instability is augmented by a portion proportional to the applied shear rate. No destabilizing mechanism for well aligned parallel layers is present in the standard smectic-A hydrodynamics.

Recently, we proposed an extended hydrodynamic description [25,26] of smectic-A liquid crystals. Using both, the

---

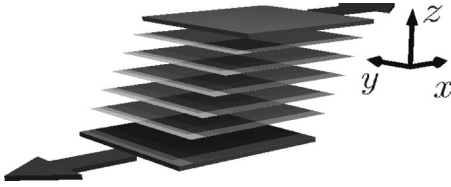*Electronic address: guenter.auernhammer@uni-bayreuth.de

FIG. 1. At the level of the approximation we use in this paper, all experimental shear geometries are equivalent to a simple steady shear. We choose our system of coordinates such that the normal to the plates points along the z axis and the plates are located at $z = \pm d/2$.

director of the underlying nematic order and the layer normal of the smectic layers, we showed the possibility of a shear-induced undulation instability in well aligned parallel layers. Within the framework of irreversible thermodynamics (which allows the inclusion of dissipative as well as reversible effects) we derived macroscopic hydrodynamic equations for the system and performed a linear stability analysis of these equations (using a number of approximations). As always, a linear stability analysis is limited to the onset of the first instability. Other theoretical approaches to these reorientation phenomena have been undertaken by Bruinsma and Rabin [27], Zilman and Granek [28] (both papers consider the influence of the shear on layer fluctuations) and Williams and MacKintosh [29] (minimizing a free energy density including a coupling to the applied shear stress). To our knowledge, no macroscopic hydrodynamic approach besides Refs. [25,26] has been published up to now.

The present paper is structured as follows. After a brief review of the model in Sec. II A and its implementation in Sec. II B we extend the basic model of Refs. [25,26] in the following sections. Especially, we include the cross coupling to the velocity field and the moduli of the nematic and smectic order parameters. It turns out that the coupling terms to the velocity are important since they can change the critical parameters significantly. We find that the moduli of the order parameters also show undulations and, thus, regions with a reduced order parameter can be identified. The comparison of the different levels of approximations shows that the basic model is contained in this more general analysis as a special case. We also compare our results to experiments and molecular dynamic simulations and show that an oscillatory instability is extremely unlikely to occur.

II. MODEL AND TECHNIQUE

A. Physical idea of the model

In a smectic-A liquid crystal one can easily define two directions: the normal to the layers $\hat{p}$ and an average over the molecular axes, the director, $\hat{n}$. In the standard formulation of smectic-A hydrodynamics, these two directions are parallel by construction. Only in the vicinity of phase transitions (either the nematic–smectic A or smectic A–smectic C^*) it has been shown that director fluctuations are of physical interest [30–32]. Nevertheless, $\hat{n}$ and $\hat{p}$ differ significantly in their interaction with an applied shear flow.

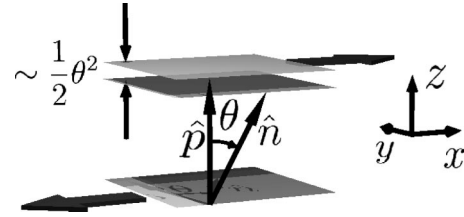We consider a situation, as shown in Fig. 1. A well

FIG. 2. A finite angle θ between $\hat{n}$ and $\hat{p}$ leads to a tendency of the layers to reduce their thickness. Supposing a constant number of layers in the sample, this tendency is equivalent to an effective dilatation of the layers. For small angles between $\hat{n}$ and $\hat{p}$ the relative effective dilation is given by $\theta^2/2$.

aligned smectic-A liquid crystal is placed between two parallel and laterally infinite plates. The upper plate (located at $z = d/2$) moves with a constant velocity $\vec{v}_u = d\dot{\gamma}\hat{e}_x/2$ to the right and the lower plate (at $-d/2$) moves with the same velocity in the opposite direction ($\vec{v}_l = -d\dot{\gamma}\hat{e}_x/2$). Thus the sample is submitted to an average shear given by ($v_u - v_l)/d = \dot{\gamma}$. As mentioned above, a three-dimensional stack of parallel fluid layers cannot couple directly to an applied shear flow. Neither does the layer normal: it stays unchanged as long as the flow direction lies within the layers. In contrast, it is well known from nematic hydrodynamics that the director experiences a torque in a shear flow. This torque leads—in the simplest case—to a flow aligning behavior of the director. The key assumption in the model of Ref. [25] is that this torque is still present in a smectic-A liquid crystal and acts only on the director $\hat{n}$ and not on the layer normal $\hat{p}$. An energetic coupling between $\hat{n}$ and $\hat{p}$ ensures that both directions are parallel in equilibrium.

Submitted to a shear flow, the layer normal will stay unchanged, but the director will tilt in the direction of the flow until the torques due to the flow and due to the coupling to the layer normal balance one another. For any given shear rate a finite, but usually small, angle θ between $\hat{n}$ and $\hat{p}$ will result. This finite angle has important consequences for the layers. Since the preferred thickness of the layers is proportional to the projection of the director on the layer normal, a finite angle between those two directions is equivalent to an effective dilatation of approximately $\theta^2/2$ (see Fig. 2). If we assume a constant total sample thickness and exclude effects of defects, the system can accommodate this constraint by layer rotations. A global rotation of the layers is not possible, but they can rotate locally (as in the case of dilated smectic A liquid crystals [21,22]). This local rotation of the layers leads to undulations, as shown in Fig. 3. These undulations are a compromise between the effective dilatation (which is not favorable for the system) and the curvature of the layers due to the undulations (which costs energy). In the static case of dilated smectic-A liquid crystals no direction is preferred, but Oswald and Ben-Abraham [23] have shown that this symmetry is broken if an additional shear is applied to the system. In this case, the standard formulation of smectic-A hydrodynamics predicts that the wave vector of the undulations will point along the neutral direction of the shear. In this paper we will assume that this result of Oswald and Ben-Abraham
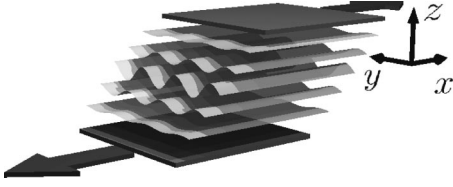
FIG. 3. Above a certain threshold the effective dilatation due to the director tilt will lead to buckling of the layers. Note the difference in directions: the director is tilted in the flow direction, whereas the wave vector points along the y axis. This configuration cancels the direct coupling between the flow and the buckling.

also holds in the case of our extended formulation of smectic-A hydrodynamics (see Fig. 3).

B. Implementation of the model

To generate the macroscopic hydrodynamic equations we follow the procedure given by the framework of irreversible thermodynamics [33]. This method has successfully been applied in many cases to derive the macroscopic hydrodynamic equations of complex fluids (see, e.g., Refs. [18,20,25,34]). The advantage of this method is its systematic way of deducing the governing equations. Once the set of variables is given, the macroscopic hydrodynamic equations follow by applying basic symmetry arguments and thermodynamic considerations.

Let us briefly review the essential ingredients to this procedure (for more details of the method, see Ref. [20], and for our model, see Ref. [25]). For a given system the hydrodynamic variables can be split up in two categories: variables reflecting conserved quantities (e.g., the linear momentum density, the mass density, etc.) and variables due to spontaneously broken continuous symmetries (e.g., the nematic director or the layer displacements of the smectic layers). Additionally, in some cases, nonhydrodynamic variables (e.g., the strength of the order parameter [35]) can show slow dynamics that can be described within this framework (see, e.g., Refs. [20,34]).

Using all these variables, the relations, which form the starting point for the further calculations, can be constructed. These relations are: the energy density ϵ, the dissipation function R, the Gibbs relation-, and the Gibbs-Duhem relation. To illustrate the idea of our model, we split up ϵ and R into several parts according to the different origin of the variables: conserved quantities (index $cons$), symmetry variables (index sym), and the modulus of the order parameter (index ord), In the spirit of our model, two order parameters play a role: the nematic tensorial order parameter Q_{ij} and the smectic-A complex order parameter Φ. For practical reasons we use the director $\hat{n}$ and the modulus $S^{(n)}$ in the uniaxial nematic case $[Q_{ij}=\frac{3}{2}S^{(n)}(n_i n_j - \frac{1}{3}\delta_{ij})]$ and the layer displacement u and the modulus $S^{(s)}$ in the smectic-A case $[\Phi=S^{(s)}\exp\{iq_0(z-u)\}]$. Here, as in the rest of the paper, we refer to the system of coordinates defined in Sec. II A. We note that u is only a good variable if we consider small deformations of the layers. For large layer deformations the phase $\varphi=z-u$ is the appropriate variable [36,37]. In our further discussion, we will concentrate on the parts due to

TABLE I. Summary of the notation. In these definitions we use the transverse Kronecker symbol $\delta_{ij}^{\perp}=\delta_{ij}-n_i n_j$. Due to the thermodynamic stability of the systems, the following combinations of constants must be positive: B_0, B_1, K, L_0, $L_{\perp}^{(n,s)}$, $L_{\parallel}$, and $M_0^2 - KL_{\parallel}$. For the last relation we used the equivalence of K and K_1.

Symbol	Explicit form	Comment
K	K	Bending modulus of layers
B_0	B_0	Compressibility of layers
B_1	B_1	Coupling between the director and the layer normal
$L_0^{(n,s)}$	$L_0^{(n,s)}$	Variations of the order parameter (nematic and smectic, respectively)
$L_{1,ij}^{(n)}$	$L_{\perp}^{(n)}\delta_{ij}^{\perp}+L_{\parallel}^{(n)}n_i n_j$	Gradient terms of the order parameter (nematic)
M_{ijk}	$M_0(\delta_{ij}^{\perp}n_k+\delta_{ik}^{\perp}n_j)$	Cross coupling between the director and order parameter (nematic)
$L_{1,ij}^{(s)}$	$L_{\perp}^{(s)}(\delta_{ij}-p_i p_j)$ $+L_{\parallel}^{(s)}p_i p_j$	Gradient terms of the order parameter (smectic)

symmetry variables and the order parameters, while for terms already present in the isotropic fluid see, e.g., Refs. [20,33].

Let us first consider the energy density. The conventions of notation introduced by the following equations are summarized in Table I.

$$\epsilon=\epsilon_{cons}+\epsilon_{sym}+\epsilon_{ord}^{(n)}+\epsilon_{ord}^{(s)}, \quad (1)$$

ϵ_{cons}, which is identical to the isotropic fluid, is discussed elsewhere [20,33]. The symmetry part reads,

$$\epsilon_{sym}=\frac{1}{2}K_1(\nabla\cdot\hat{n})^2+\frac{1}{2}K_2[\hat{n}\cdot(\nabla\times\hat{n})]^2$$

$$+\frac{1}{2}K_3[\hat{n}\times(\nabla\times\hat{n})]^2$$

$$+\frac{1}{2}K(\nabla_{\perp}^2 u)^2$$

$$+\frac{1}{2}B_0\left[\nabla_z u+(1-n_z)-\frac{1}{2}(\nabla_{\perp}u)^2\right]^2$$

$$+\frac{1}{2}B_1(\hat{n}\times\hat{p})^2. \quad (2)$$

In Eq. (2) the spirit of the model becomes clear. We combine the properties of a nematic liquid crystal (the first two lines) with these of a smectic A (the third and fourth line) and couple both parts (the last line) in such a way that $\hat{n}$ and $\hat{p}$ are parallel in equilibrium. As already discussed earlier [25], ϵ_{sym} simplifies considerably by dropping higher-order terms and assuming a small angle between $\hat{n}$ and $\hat{p}$. Splay deformations of the director are generally considered as higher-order corrections to dilatations of the smectic layers. Twist deformations are forbidden in standard smectic-A hydro

TABLE II. Variables and their conjugates, i.e., the corresponding thermodynamic forces.

Name	Variable	Conjugate
Mass density	ρ	μ
Momentum density	$\vec{g}$	$\vec{v}$
Nematic director	$\hat{n}$	$\vec{h}$
Smectic layer displacement	u	Ψ
Variation of the modulus of the order parameter (either nematic or smectic)	$s^{(n,s)}$	$\Xi^{(n,s)}$

namics and must be small as long as the angle between $\hat{n}$ and $\hat{p}$ is small. Additionally, the difference between the splay deformation of the director field $K_1/2(\nabla \cdot \hat{n})^2$ and bending of the layers $K/2(\nabla_\perp^2 u)^2$ is negligible. Consequently, we combine splay and bend in a single term with a single elastic constant which we call K': $K_1/2(\nabla \cdot \hat{n})^2 + K/2(\nabla_\perp^2 u)^2 \approx K'/2(\nabla_\perp^2 u)^2$. In the following, we drop the prime and call the new elastic constant K. The approximated version of ϵ_{sym} is now given by

$$\epsilon_{sym} = \frac{1}{2}K(\nabla_\perp^2 u)^2 + \frac{1}{2}B_0\left[\nabla_z u + (1-n_z) - \frac{1}{2}(\nabla_\perp u)^2\right]^2$$
$$+ \frac{1}{2}B_1(\hat{n} \times \hat{p})^2. \qquad (3)$$

In our model the moduli of the nematic and smectic order parameters play similar roles, so we will deal with both. Since we consider a situation beyond the phase transition regime, the equilibrium value of the order parameter is nonzero ($S_0^{(n,s)}$, for both nematic and smectic) and only its variations $s^{(n,s)}$ can enter the energy density ($S^{(n,s)} = S_0^{(n,s)} + s^{(n,s)}$),

$$\epsilon_{ord}^{(n)} = \frac{1}{2}L_0(s^{(n)})^2 + \frac{1}{2}L_{1,ij}^{(n)}(\nabla_i s^{(n)})(\nabla_j s^{(n)}) + M_{ijk}\nabla_j n_i \nabla_k s^{(n)}, \qquad (4)$$

$$\epsilon_{ord}^{(s)} = \frac{1}{2}L_0(s^{(s)})^2 + \frac{1}{2}L_{1,ij}^{(s)}(\nabla_i s^{(s)})(\nabla_j s^{(s)}). \qquad (5)$$

By a similar construction we write down the dissipation function as (see Table II for a list of the thermodynamic variables and their conjugates)

$$R = R_{cons} + R_{sym} + R_{ord}, \qquad (6)$$

$$R_{cons} = \frac{1}{2}\nu_{ijkl}(\nabla_j v_i)(\nabla_l v_k) + R_0, \qquad (7)$$

$$R_{sym} = \frac{1}{2\gamma_1}h_i\delta_{ij}^\perp h_j + \lambda_p\Psi^2, \qquad (8)$$

$$R_{ord} = \frac{1}{2}\alpha^{(n)}\Xi^{(n)2} + \frac{1}{2}\alpha^{(s)}\Xi^{(s)2}, \qquad (9)$$

where R_0 summarizes further terms due to conservations laws, which do not enter our further calculation, and (after Ref. [38])

$$\nu_{ijkl} = \nu_2(\delta_{jl}\delta_{ik} + \delta_{il}\delta_{jk})$$
$$+ 2(\nu_1 + \nu_2 - 2\nu_3)n_i n_j n_k n_l$$
$$+ (\nu_3 - \nu_2)(n_j n_l \delta_{ik} + n_j n_k \delta_{il}$$
$$+ n_i n_k \delta_{jl} + n_i n_l \delta_{jk})$$
$$+ (\nu_4 - \nu_2)\delta_{ij}\delta_{kl}$$
$$+ (\nu_5 - \nu_4 + \nu_2)(\delta_{ij}n_k n_l + \delta_{kl}n_i n_j). \qquad (10)$$

As mentioned in Sec. II A we consider a shear induced smectic-C-like situation (but with a small tilt angle, i.e., a weak biaxiality). We neglect this weak biaxiality in the viscosity tensor and use it in the uniaxial formulation given above (with the director $\hat{n}$ as the preferred direction). This assumption is justified by the fact that the results presented in this paper do not change significantly if we use $\hat{p}$ instead of $\hat{n}$ in the viscosity tensor.

Throughout our calculations, we will not assume any restriction on the viscosity constants except the usual requirements due to thermodynamic stability (see, e.g., Ref. [20]). Later on, we will impose the incompressibility of the fluid by assuming a constant mass density ρ of the fluid. We emphasize that this procedure does not require any further assumption about the material parameters.

The set of basic equations is completed by the Gibbs-Duhem relation (the local formulation of the second law of thermodynamics) and the Gibbs relation (which connects the pressure P with the other thermodynamic quantities), which we will use in the following form:

$$d\epsilon = d\epsilon_0 + \vec{v} \cdot d\vec{g} + \varphi_{ij}d\nabla_j n_i + h_i' dn_i + \Xi'^{(n)}ds^{(n)}$$
$$+ \Xi_i''^{(n)}d\nabla_i s^{(n)} + \Xi'^{(s)}ds^{(s)} + \Xi_i''^{(s)}d\nabla_i s^{(s)}, \qquad (11)$$

$$P = -\epsilon + \mu\rho + T\sigma + \vec{v} \cdot \vec{g}. \qquad (12)$$

The newly defined quantities in Eq. (11) are connected to the thermodynamic forces (Table II) by the following relations:

$$h_i = h_i' - \nabla_j \varphi_{ij} = \frac{\delta\epsilon}{\delta n_i}, \qquad (13)$$

$$\Psi = -\nabla_i \psi_i = \frac{\delta\epsilon}{\delta u}, \qquad (14)$$

$$\Xi^{(n,s)} = \Xi'^{(n,s)} - \nabla_i \Xi_i''^{(n,s)} = \frac{\delta\epsilon}{\delta s^{(n,s)}}. \qquad (15)$$

Following the standard procedure within the framework of irreversible thermodynamics we find the following set of macroscopic hydrodynamic equations [20,25,33,34],

$$\frac{\partial}{\partial t}u + v_j\nabla_j u = v_z - \lambda_p\Psi, \qquad (16)$$

$$\frac{\partial}{\partial t}n_i+v_j\nabla_j n_i=\frac{1}{2}[(\lambda-1)\delta^\perp_{ij}n_k+(\lambda+1)\delta^\perp_{ik}n_j]\nabla_j v_k$$

$$-\frac{1}{\gamma_1}\delta^\perp_{ik}h_k, \tag{17}$$

$$0=\nabla_i v_i, \tag{18}$$

$$\rho\left(\frac{\partial}{\partial t}v_i+v_j\nabla_j v_i\right)=-\nabla_j\left\{\psi_j(\nabla_i u+\delta_{i3})+\beta^{(n,s)}_{ij}\Xi^{(n,s)}\right.$$

$$-\frac{1}{2}[(\lambda-1)\delta^\perp_{jk}n_i+(\lambda+1)\delta^\perp_{ik}n_j]h_k$$

$$\left.+\nu_{ijkl}\nabla_l v_k\right\}-\nabla_i P, \tag{19}$$

$$\frac{\partial}{\partial t}s^{(n,s)}+v_j\nabla_j s^{(n,s)}=-\beta^{(n,s)}_{ij}\nabla_j v_i-\alpha^{(n,s)}\Xi^{(n,s)}. \tag{20}$$

For the reversible parts of the equations some coupling constants have been introduced. The flow-alignment tensor

$$\lambda_{ijk}=\frac{1}{2}[(\lambda-1)\delta^\perp_{ij}n_k+(\lambda+1)\delta^\perp_{ik}n_j], \tag{21}$$

with the flow-alignment parameter λ (and using $\delta^\perp_{ij}=\delta_{ij}-n_i n_j$) and the coupling between flow and order parameter,

$$\beta^{(n)}_{ij}=\beta^{(n)}_\perp\delta^\perp_{ij}+\beta^{(n)}_\parallel n_i n_j, \tag{22}$$

$$\beta^{(s)}_{ij}=\beta^{(s)}_\perp(\delta_{ij}-p_i p_j)+\beta^{(s)}_\parallel p_i p_j. \tag{23}$$

Furthermore, there is a reversible coupling between the layer displacement and the velocity field in Eq. (16). But its coupling constant has to be unity due to the Gallilei invariance of the equations. As mentioned above, the use of u is limited to small layer deformations.

The transverse Kronecker symbols $\delta^\perp_{ij}$ in Eqs. (17) and (21) guarantee the normalization of $\hat{n}$. This implies that only two of the Eqs. (17) are independent. For the following calculations it turned out to be useful to guarantee the normalization of the director by introducing two angular variables θ and ϕ to describe the director,

$$n_x=\sin\theta\cos\phi, \tag{24}$$

$$n_y=\sin\theta\sin\phi, \tag{25}$$

$$n_z=\cos\theta. \tag{26}$$

Consequently, Eqs. (17) have to be replaced using angular variables. Denoting the right-hand side of Eqs. (17) with Y_i, this can be done the following way:

$$\frac{\partial}{\partial t}\theta+v_j\nabla_j\theta=Y_x\cos\theta\cos\phi+Y_y\cos\theta\sin\phi-Y_z\sin\theta, \tag{27}$$

$$\frac{\partial}{\partial t}\phi+v_j\nabla_j\phi=-Y_x\frac{\sin\phi}{\sin\theta}+Y_y\frac{\cos\phi}{\sin\theta}. \tag{28}$$

In the same way, we guarantee the normalization of $\hat{p}$ by using

$$p_x=0, \tag{29}$$

$$p_y=-\nabla_y u, \tag{30}$$

$$p_z=\sqrt{1-p_y^2}. \tag{31}$$

The different ways of normalizing $\hat{n}$ and $\hat{p}$ arise from the fact that $\hat{p}$ is parallel to $\hat{e}_z$ in zeroth order, whereas $\hat{n}$ encloses a finite angle with $\hat{e}_z$ for any given shear rate.

The set of macroscopic hydrodynamic equations we now deal with (16),(18)–(20),(27),(28) follows directly from the initial input in the energy density and the dissipation function without any further assumptions.

To solve these equations we need suitable boundary conditions. In the following we will assume that the boundaries have no orienting effect on the director (the homeotropic alignment of the director is only due to the layering and the coupling between the layer normal $\hat{p}$ and the director $\hat{n}$). Any variation of the layer displacement must vanish at the boundaries,

$$u\left(\pm\frac{1}{2}d\right)=0. \tag{32}$$

For the velocity field the situation is a little more complex. We assume no-slip boundary conditions, i.e., the velocity of the fluid and the velocity of the plate are the same at the surface of the plate. It is convenient to split the velocity field in two parts: the shear field $\vec{v}_0$ which satisfies the governing equations and the no-slip boundary condition and the correction $\vec{v}_1$ to this shear field. The boundary condition for $\vec{v}_1$ now reads,

$$\vec{v}_1\left(\pm\frac{1}{2}d\right)=0. \tag{33}$$

Making use of the following considerations this condition can be simplified. Due to Eq. (16) the z component of $\vec{v}_1$ is suppressed by a factor of λ_p (which is typically extremely small [19,23]). Making use of the results of Ref. [23] we can assume that $\vec{v}_1$ depends only on y and z and thus conclude [with Eq. (18)] that the y component of $\vec{v}_1$ is also suppressed by λ_p. For this reason, one can assume that $v_{1,y}$ and $v_{1,z}$ are negligible and the only relevant boundary condition for the velocity field is

$$v_{1,x}=0. \tag{34}$$

The validity of this assumption is nicely illustrated by our results. Figure 7 shows that v_y and v_z are indeed suppressed by λ_p.

TABLE III. If the symmetry under inversion of z is given for one component of $\vec{X}_1$, the symmetry of all other components follows directly from the linearized set of equations. Here we give the z symmetry of all components, assuming that u is an even function of z.

Quantity	z symmetry	Quantity	z symmetry
u	Even	v_x	Even
θ	Odd	v_y	Odd
ϕ	Even	v_z	Even
P	Odd	$s^{(n,s)}$	Odd

C. Technique of solution

The aim now is twofold. Finding a spatially homogeneous solution of the governing equations (for a given shear rate) and investigating the stability of this solution. In this section we will describe the general procedure and give the results in Sec. III.

We write the solution as the vector $\vec{X} = (\theta, \phi, u, v_x, v_y, v_z, P, s^{(n,s)})$ consisting of the angular variables of the director, the layer displacement, the velocity field, the pressure, and the modulus of the (nematic or smectic) order parameter. For a spatially homogeneous situation the equations simplify significantly and the desired solution $\vec{X}_0$ can directly be found (see Sec. III A). To determine the region of stability of $\vec{X}_0$ we perform a linear stability analysis. That is, we add a small perturbation $\vec{X}_1$ to the homogeneous solutions X_0: $\vec{X} = \vec{X}_0 + \vec{X}_1$ (with $\vec{X}_1 \ll \vec{X}_0$) and linearize the governing equations in the small perturbations. In short, the solution of the equation $\mathsf{L}\vec{X}_1 = \partial/\partial t \vec{X}_1$ is analyzed. Here L denotes the operator for the linearized set of the governing equations. The ansatz for the unknown quantities must fulfill the boundary conditions [see the discussion following Eq. (32)] and follow the symmetry scheme given by Table III. Assuming an exponential time dependence and harmonic spatial dependence of $\vec{X}_1$,

$$X_{1,i} \sim \exp\left[\left(i\omega + \frac{1}{\tau}\right)t\right] \begin{Bmatrix} \cos(qy) \\ \sin(qy) \end{Bmatrix} \begin{Bmatrix} \cos(q_z z) \\ \sin(q_z z) \end{Bmatrix}, \quad (35)$$

fulfills all requirements (with an oscillation rate ω, a growth rate $1/\tau$, and a wave vector $\vec{q} = q\hat{e}_y + q_z\hat{e}_z$). In this ansatz we made use of the results of Oswald and Ben-Abraham [23], who have shown that in standard dilated smectic A under shear the first instability will set in with a wave vector along the neutral direction of the flow ($\vec{q} \cdot \hat{e}_x = 0$). After inserting the above ansatz in the linearized set of (partial differential) equations, a set of coupled linear equations is obtained to determine $1/\tau$ and ω. From the standard smectic-A hydrodynamics it is known that shear does not destabilize the layers. Since our extended formulation of the smectic-A hydrodynamics is equivalent to the standard smectic-A hydrodynamics for vanishing external fields (e.g., shear rate), we assume that the layers are stable for low enough shear rates, i.e., $1/\tau < 0$ for small shear rates. So $1/\tau = 0$ marks the set of

external parameters (shear rate) and material parameters above which $\vec{X}_1$ grows. Typically we hold the material parameters fixed and the only external parameter is the shear rate. The solvability condition of the corresponding set of linear equations gives a relation between the shear rate [and tilt angle θ_0, which is directly connected to the shear rate, see Eq. (38) below], ω, and the wave vector q. For every given q a specific shear rate (and tilt angle θ_0) can be determined which separates the stable region (below) from the unstable region (above). This defines the so called curve of marginal stability (or neutral curve) $\theta_0(q)$. If, for any given set of external parameters, the tilt angle θ_0 lies above the curve of marginal stability for at least one value of q, the spatial homogeneous state is unstable and undulations grow. The smallest shear rate (tilt angle) for which undulations can grow is called the critical shear rate (tilt angle). Technically speaking, we solve $\mathsf{L}\vec{X} = i\omega\vec{X}$—in many cases we can set $\omega = 0$, see below. We point out that this linear analysis is only valid at the point where the first instability sets in. Without further investigations no prediction of the spatial structure of the developing instability can be made. Also, the nature of the bifurcation (backward or forward) must be determined by further investigations.

For practical reasons we used dimensionless units in our numerical calculations. The invariance of the governing equations under rescaling time, length, and mass allows us to choose three parameters in these equations to be equal to unity. We will set

$$B_1 = 1, \quad \gamma_1 = 1, \quad \text{and} \quad \frac{d}{\pi} = q_z = 1 \quad (36)$$

and measure all other quantities in the units defined by this choice. Nevertheless, we will keep these quantities explicitly in our analytical work.

To extract concrete predictions for experimental parameters from our calculations is a nontrivial task, because neither the energetic constant B_1 nor the rotational viscosity γ_1 are used for the hydrodynamic description of the smectic-A phase (but play an important role in our model). Therefore, we here rely on measurements in the vicinity of the nematic–smectic-A phase transition. Measurements on low molecular weight liquid crystals made by Litster [31] in the vicinity of the nematic–smectic-A transition indicate that B_1 is approximately one order of magnitude less than B_0. As for γ_1, we could not find any measurements that would allow an estimate of its value in the smectic-A phase. In the nematic phase γ_1 increases drastically towards the nematic–smectic-A transition (see, e.g., Ref. [39]). Numerical simulations on a molecular scale are also a promising approach to determine these constants [40].

Due to the complexity of the full set of governing equations, we will start our analysis with a minimal set of variables (θ, ϕ, and u) and suppress the coupling to the other variables (see Sec. III B 1). Step by step, the other variables will be taken into account. The general picture of the instability will turn out to be already present in the minimal model, but many interesting details will be added throughout

the next sections. In comparison to our earlier work [25] we now use the way of normalizing $\hat{n}$ and $\hat{p}$ derived above. This will lead to some small differences in the results but leaves the general picture unchanged. First we assume a stationary instability (i.e., we let $\omega=0$); later on we discuss the possibility for an oscillatory instability and have a look at some special features of the system (Secs. III C and III D).

III. RESULTS AND DISCUSSION

A. Spatially homogeneous state

Looking for a spatially homogeneous solution, the governing equations simplify significantly. A linear shear profile

$$\vec{v}_0 = \dot{\gamma} z \hat{e}_x \tag{37}$$

is a solution to Eq. (19) and u stays unchanged in this regime. The only variables that have a zeroth order correction for all shear rates are the tilt angle θ and the modulus of the nematic order parameters $s^{(n)}$,

$$\left(\frac{\lambda+1}{2} - \lambda \sin^2(\theta_0)\right) \dot{\gamma} = \frac{B_1}{\gamma_1} \sin(\theta_0)\cos(\theta_0)$$
$$+ \frac{B_0}{\gamma_1} \sin(\theta_0)[1 - \cos(\theta_0)], \tag{38}$$

$$\alpha^{(n)} L_0 s_0^{(n)} = (\beta_\parallel^{(n)} - \beta_\perp^{(n)}) \sin(\theta_0)\cos(\theta_0) \dot{\gamma}. \tag{39}$$

Equation (39) shows that nematic degrees of freedom couple to simple shear, but not the smectic degrees of freedom; the modulus of the nematic order parameter has a nonvanishing spatially homogeneous correction [see Eq. (39)], whereas the smectic order parameter stays unchanged. The reason for this difference lies in the fact that $\beta_{ij}^{(n)}$ and $\beta_{ij}^{(s)}$ include $\hat{n}$ and $\hat{p}$, respectively, which coupled differently to the flow field [see Eqs. (22) and (23)]. Equation (38) gives a well defined relation between the shear rate $\dot{\gamma}$ and the director tilt angle θ_0, which we will use to eliminate $\dot{\gamma}$ from our further calculations. To lowest order, θ_0 depends linearly on $\dot{\gamma}$,

$$\theta_0 = \dot{\gamma} \frac{\gamma_1}{B_1} \frac{\lambda+1}{2} + O(\theta_0^3). \tag{40}$$

We are not aware of any experimental data, which would allow a direct comparison with these results. We stress, however, that molecular dynamics simulations by Soddemann *et al.* [40] are in very good agreement with Eqs. (38) and (40).

In contrast to the director tilt, the lowest-order correction to the nematic order parameter is quadratic in the shear rate (tilt angle),

$$s_0^{(n)} = \frac{2}{\lambda+1} \frac{B_1}{\gamma_1} \frac{\beta_\parallel^{(n)} - \beta_\perp^{(n)}}{\alpha^{(n)} L_0} \theta_0^2 + O(\theta_0^4). \tag{41}$$

In the following we consider perturbations around the spatially homogeneous state given above.

B. Stationary instability

1. Minimal set of variables

Let us first consider the effect of our modifications regarding the normalization of $\hat{n}$ and $\hat{p}$ in comparison to our earlier results [25]. For this purpose we consider only a minimal set of variables: the director (characterized by the two angles θ and ϕ) and the layer displacement u. We neglect all couplings of these variables to other quantities describing the system, namely, the velocity field and the moduli of the nematic and smectic order parameters. Within these approximations the equations to solve are,

$$0 = A_\theta \left\{ 2\dot{\gamma}\lambda \sin(\theta_0)\cos(\theta_0) + \frac{B_0}{\gamma_1}[\sin^2(\theta_0) - \cos^2(\theta_0)] \right.$$
$$\left. + \cos(\theta_0)] - \frac{B_1}{\gamma_1}[\sin^2(\theta_0) - \cos^2(\theta_0)] \right\}$$
$$- A_u \frac{B_0}{\gamma_1} \sin(\theta_0) q_z, \tag{42}$$

$$0 = A_\phi \frac{1}{2}\dot{\gamma}(\lambda+1) - A_u \frac{B_1}{\gamma_1} q, \tag{43}$$

$$0 = A_\theta \lambda_p B_0 \sin(\theta_0) q_z + A_\phi \lambda_p B_1 q \sin(\theta_0)\cos(\theta_0)$$
$$- A_u \lambda_p [-B_0 q^2[1 - \cos(\theta_0)] + B_1 q^2 \cos^2(\theta_0)$$
$$+ K q^4 + B_0 q_z^2]. \tag{44}$$

Here we inserted an ansatz of the type (35) and denoted the linear amplitudes of θ, ϕ, and u by A_θ, A_ϕ, and A_u, respectively. One can solve these equations either by expanding them in a power series of θ_0 (expecting to get a closed result for the critical values) or numerically. It turns out, that one has to take into account terms (at least) up to order θ_0^5 in Eqs. (42)–(44) to get physically meaningful (but rather long and complicated) analytical results. For this reason the closed expressions have no advantage over the purely numerical solutions and we do not give the analytical approximations explicitly. A comparison with the results of Ref. [25] will be given in Appendix A. We will present and discuss our findings using the minimal set of variables in Sec. III B 2, in direct comparison to the results of the full set of equations.

2. Coupling to the velocity field

In the preceding section we have shown that already a minimal set of variables supports our picture of the physical mechanism. But neglecting the coupling between velocity field and nematic director and vice versa is a rather crude approximation since it is well known that this coupling plays an important role in nematic hydrodynamics [19,20]. So the natural next step is to include this coupling and to perform a linear stability analysis of Eqs. (16)–(19), (27),(28). In this case, the standard procedure leads to a system of seven
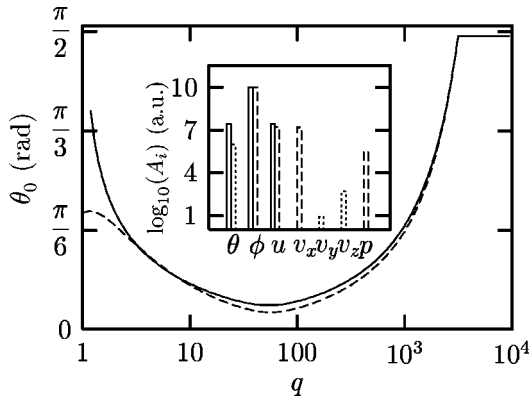
FIG. 4. A typical picture for the comparison of the neutral curves using the minimal set of variables (——) and including the velocity field ($-\,-\,-$). The overall behavior does not change, but the critical values are altered due to the coupling with the velocity field. For this plot we used (in the dimensionless units discussed in Sec. II C) $B_0 = 10$, $K = 10^{-6}$, $\lambda = 1.1$, $\nu_1 = \nu_2 = \nu_3 = \nu_4 = \nu_5 = 0.1$, and $\lambda_p = 10^{-6}$. The inset shows the linear amplitudes A_i (where i stands for θ, ϕ, etc) at onset. Since the logarithm of the amplitudes is shown, amplitudes with different sign are shown with a different line style. Using the minimal set (left bars) all amplitudes have the same sign (——). Including the velocity field (right bars) some amplitudes are positive ($-\,-\,-$), others negative (. . .). Note that we use in this and all following plots the dimensionless units defined by Eq. (36).

coupled linear differential equations. Following the discussion after Eq. (32) these equations can be solved by an ansatz of the type given in Eq. (35). This reduces the system of equations to seven coupled linear equations which are easily solved using standard numerical tools (such as singular value decomposition and inverse iteration to find the eigenvectors). Due to the complexity of the equations, we used Maple to determine the final set of linear equations. The key ingredients of this Maple script are given in Appendix B.

Figure 4 gives a comparison of typical neutral curves for the minimal model and calculations including the velocity field. The overall shape of the neutral curve is not changed due to the coupling to the velocity field but a shift of the
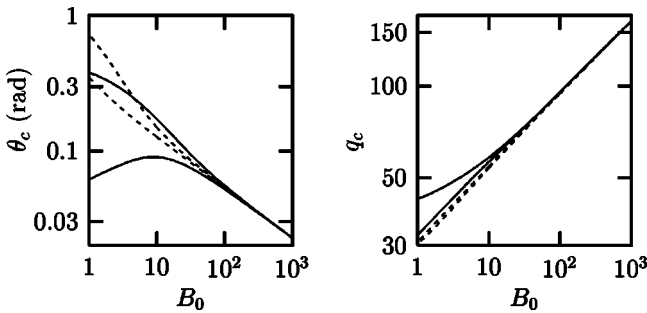

FIG. 5. A significant difference between the various approaches is only visible for $B_0 \lesssim 100$. At higher values of B_0 the number of free variables plays no noticeable role and the critical values follow a master curve. The solid lines (——) show results including the velocity field, the dashed lines ($-\,-\,-$) correspond to the minimal set of variables. At low B_0 in the upper curves we used $\lambda = 2$.
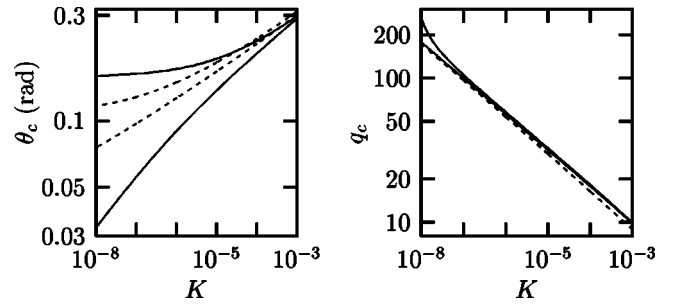

FIG. 6. Plotting the critical values as a function of the bending modulus K shows a convergence of the curves, which is, nevertheless, not as pronounced as in the case of Fig. 5. The influence of λ on the critical tilt angle is significant ($\lambda = 2$ in the upper curves and $\lambda = 1.1$ in the lower ones). Again the solid lines (——) show results including the velocity field and the dashed lines ($-\,-\,-$) correspond to the minimal set of variables.

critical values (especially in the critical tilt angle) is already visible. The inset shows the relative amplitudes of the linear solutions at onset on a logarithmic scale. For θ, ϕ, and u the left bars correspond to the minimal model and the right bars to the extended version. Note that amplitudes with a different sign are shown with a different line style in the histograms (see figure caption for details).

Let us have a closer look at the differences between the minimal and the extended set of equations and follow these differences along some paths in the parameter space. As mentioned in Sec. II C, we can omit some of the physical parameters by using dimensionless parameters. In Figs. 5–9 we show the dependence of the critical values of the tilt angle and wave vector on the dimensionless parameters [as defined in Eq. (36)]. For all these figures we used the same basic set of parameters: $B_0 = 10$, $K = 10^{-6}$, $\lambda = 1.1$, $\nu_1 = \nu_2 = \nu_3 = \nu_4 = \nu_5 = 0.1$, and $\lambda_p = 10^{-6}$. These values are estimates for a typical thermotropic LMW liquid crystal, where we made use of the results of Refs. [31,39] (as far as B_1 and γ_1 are concerned, see also the last paragraph in Sec. III B 1). For flow alignment parameters in the range $1 \lesssim \lambda \lesssim 3$ the critical values vary strongly with λ (see Fig. 9). Therefore we discuss in addition the situation for $\lambda = 2$ to indicate the range of possible values.
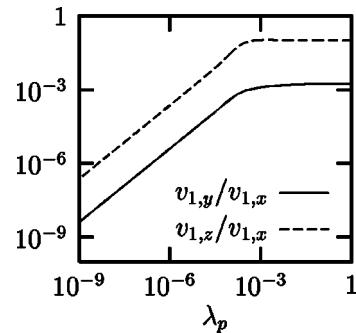

FIG. 7. In all our calculations $v_{1,x}$ is the dominating component of $\vec{v}_1$. This graph demonstrates that the other components are suppressed by λ_p (making them almost negligible).
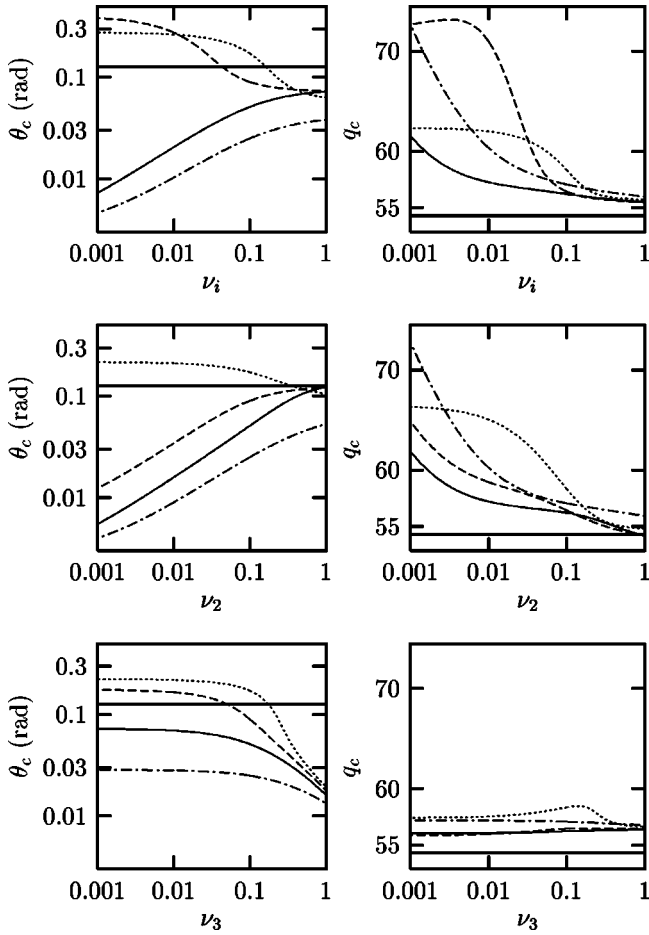
FIG. 8. Only the viscosities ν_2 and ν_3 can influence the critical parameters significantly. The upper row depicts the dependence on a isotropic variation of the viscosity. In the middle and lower row we present the variation with ν_2 and ν_3 setting the other viscosities to $\nu_i = 0.1$. Here the thick solid lines represent the minimal set of variables. For the full set of variables we have chosen four different values of λ: the thin solid curves with $\lambda = 0.7$, the dashed curves with $\lambda = 1.1$, the dotted curves with $\lambda = 2$, and the dot-dashed curves with $\lambda = 3.5$. Note the similarities between the curves for small and large λ in the upper and middle rows. In these regimes ν_2 is the dominating viscosity.

Considering the critical values as a function of the compression modulus B_0 results in a rather simple situation (Fig. 5). For small values of B_0 a significant influence of the coupling between the director and velocity field is apparent, which also shows a strong dependence on λ. For large B_0 all these differences vanish and only one single curve is obtained. At this point a comparison to dilated smectic A is instructive. It is well known [21,22] that in a dilated smectic the critical wave vector and the critical dilatation show a power law behavior as a function of B_0 with exponents 1/4 and $-1/2$, respectively. In the limit of large B_0 we found the same exponents already in our earlier analysis [25]. If we fit power laws to our results for $B_0 > 10^2$ we find the exponents equal to ≈ 0.235 and ≈ -0.37 for q_c and θ_c, respectively (note that the dilatation in our model is $\approx \frac{1}{2}\theta_c^2$). So both approaches (the minimal set of variables and the calculations
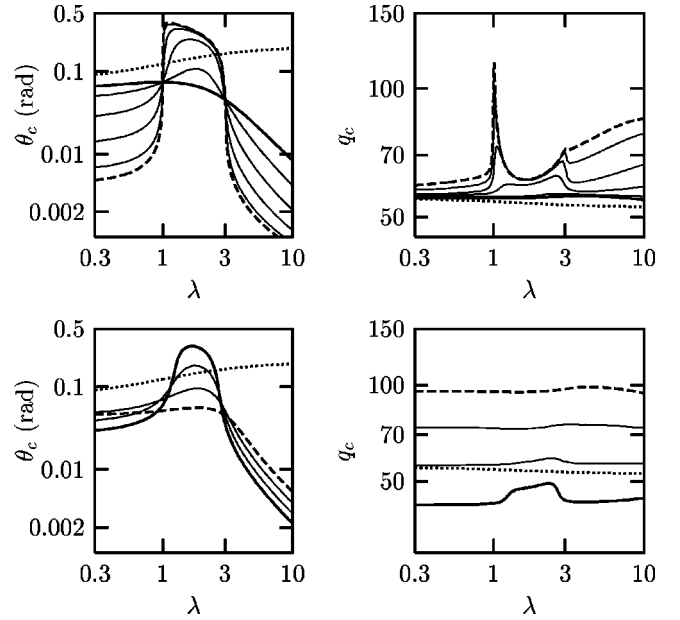
FIG. 9. Plotting the critical values as functions of the flow alignment parameter λ reveals an interesting structure for $1 \lesssim \lambda \lesssim 3$. In the upper row we plot this dependence for a set of (isotropic) viscosities ranging from $\nu_i = 1$ (thick solid line) down to $\nu_i = 10^{-3}$ (thick dashed line). The dotted line reveals that this dependence on λ is absent in the minimal model. The lower row illustrates the behavior for varying layer compressibility B_0 with $B_0 \approx 3$ for the thick solid curve and $B_0 = 100$ for the thick dashed curve. In all plots the thin solid lines give the behavior for some intermediate values. For an interpretation of this behavior see the text.

including the velocity field) show, despite all similarities to the standard model of smectic A and to our earlier analysis, differences in the details of the instability.

A similar, but less pronounced, situation is apparent, when plotting the critical values as a function of the bending modulus (see Fig. 6). The curves tend to converge for large K, but there remains a difference between the minimal set of variables and the calculations including the the velocity field. Fitting the K dependence with power laws (here for $K > 10^{-4}$) only the critical wave number exhibits an exponent close to the values expected from dilated smectic $A (\approx -0.26$ vs $-\frac{1}{4})$. This illustrates the fact that shearing a lamellar system is similar to dilating it but not equivalent.

In contrast to the cases discussed above, the permeation constant λ_p has no strong influence on the critical values. For dimensionless values $\lambda_p < 10^{-6}$ the critical values do not change at all with λ_p. For large values, variations within a factor of two are possible. The permeation constant is known to be very small. In our dimensionless units we expect it to be of the order of $< 10^{-9}$ for LMW thermotropic liquid crystals and neglect its influence on the critical values for this reason. In Sec. II B we have emphasized that the y and z components of the velocity field are suppressed via λ_p. These qualitative arguments are clearly confirmed by our numerical results: In all our calculations $v_{1,x}$ is the dominating component of $\vec{v}_1$ and the ratio $v_{1,y}/v_{1,x}$ is of the order of λ_p over the whole range of physical relevant values of λ_p (see Fig. 7). This fact nicely supports our argument that we can

neglect the boundary condition for $v_{1,y}$, because $v_{1,y}$ vanishes anyway.

Out of the five viscosities only two (ν_2 and ν_3) show a significant influence on the critical values. In Fig. 8 we present the dependence of θ_c and q_c on an assumed isotropic viscosity (upper row) and on these two viscosity coefficients (middle and lower row). Since the flow alignment parameter λ has remarkable influence on these curves, we have chosen four different values of λ in this figure, namely, $\lambda = 0.7$, $\lambda = 1.1$, $\lambda = 2$, and $\lambda = 3.5$. The curves for $\lambda \lesssim 1$ and $\lambda \gtrsim 3$ for an isotropic viscosity tensor are very similar to the corresponding curves where only ν_2 is varied. In this parameter range the coefficient ν_2 dominates the behavior. Note that the influence of ν_3 on the critical values is already much smaller than that of ν_2. We left out the equivalent graphs for the other viscosity coefficients, because they have almost no effect on the critical values. For further comments on the influence of an anisotropic viscosity tensor see also Sec. III D.

All the parameters we have discussed up to now caused variations in the critical values that did not select specific values of the considered parameter. In this aspect the situation is completely different in the case of the flow alignment parameter λ. As shown in Fig. 9, there is a clear change in behavior for $\lambda \approx 1$ and $\lambda \approx 3$. The critical tilt angle is increased for values of λ in this interval and the critical wave vector tends to rise only at the boundaries of the interval and is reduced in between. Figure 9 illustrates how this structure depends on the viscosities (assuming all five viscosities to be equal) and on the elastic constants of the layers. In the first row we follow this behavior for viscosities varying from $\nu_i = 1$ down to $\nu_i = 10^{-3}$. Clearly, the influence of λ is more pronounced the lower the viscosities are. Both elastic constants of the layers, the compressibility B_0 and the bending modulus K (in our dimensionless units $B_1 = 1$), have, in general, a similar influence on the shape of the graphs: the smaller the elastic constants are, the more pronounced the structure becomes. For this reason we just give the plot for B_0 (second row in Fig. 9) and omit the plot for K.

These dependencies on the system parameters give some important hints for an interpretation of Fig. 9. The currents and quasicurrents for the velocity field and the director consist of two parts [see Eqs. (17) and (19)]: a diagonal one (coupling, e.g., the components of $\vec{v}$ among each other) and an off-diagonal one (coupling the director to the velocity field). The former ones are proportional to the elastic constants or to the viscosity tensor, whereas the latter one is a function of the flow alignment parameter. So reducing either the elastic constants or the viscosities increases the portion of the cross-coupling terms in these equations. That is, the observed tendencies are exactly what one would expect. The next step in the interpretation of the shape of the curves is to have a closer look at the structure of the cross-coupling term. The flow alignment tensor $\lambda_{ijk} = \frac{1}{2}[(\lambda-1)\delta_{ij}^{\perp}n_k + (\lambda+1)\delta_{ik}^{\perp}n_j]$ obviously changes its behavior for $\lambda = 1$: the first part changes its sign. Note that we are in a region of the parameter space, where λ_{ijk} is a dominating term (since either the viscosities or the elastic constants are small). Additionally, $\delta_{ij}^{\perp}n_k$ contains up to the third power of one director
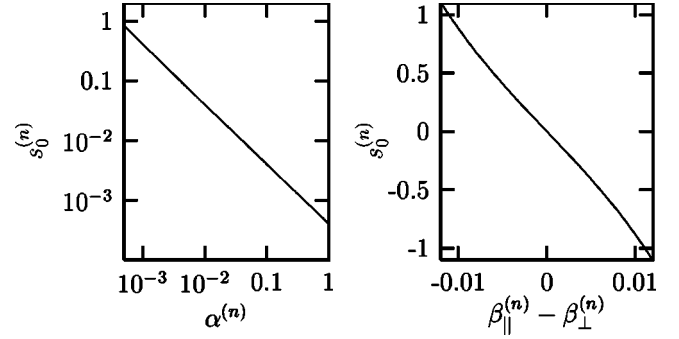

FIG. 10. Evaluating Eqs. (41) and (45) at onset gives an important restriction on the range of possible parameter values (here the cases of $\alpha^{(n)}$ and $\beta_{\parallel}^{(n)} - \beta_{\perp}^{(n)}$). Note that the critical θ_0 is a function of the material parameters.

component. For this reason, we expect that—in the linearized set of equations—some coupling terms change their sign for $\lambda = 1$, others for $\lambda = 3$. For example, the ϕ component of the director is coupled to the x and z component of the velocity field by the terms $(\lambda-1)/2\nabla_y v_x$ and $(\lambda-1)/2 \cot(\theta_0)\nabla_y v_z$. Similarly, the reversible part of the coupling of v_y to ϕ vanishes for $\lambda = 3$. The monitored structure in the plots cannot be attributed to one single cross-coupling term, but the given examples demonstrate that something should happen in this parameter range.

3. Including the order parameters

In the preceeding paragraphs we investigated undulations assuming a constant modulus of the order parameter $S^{(n,s)} = S_0^{(n,s)} + s_0^{(n,s)}$. In general, one would expect that the undulations in the other observable quantities should couple to some extent to the order parameter. In the formulation of the free energy (see Sec. II B) we have assumed that $S^{(n,s)}$ varies only slightly around $S_0^{(n,s)}$ and thus only the lowest-order terms in $s^{(n,s)}$ contribute to the free energy. For the spatially homogeneous state we had [see Eqs. (39) and (41)] a correction to the nematic $S^{(n)}$ proportional to the square of the shear rate ($\theta_0 \sim \dot{\gamma}$ for low $\dot{\gamma}$),

$$s_0^{(n)} = -\frac{2}{\lambda+1} \frac{B_1}{\gamma_1} \frac{\beta_{\parallel}^{(n)} - \beta_{\perp}^{(n)}}{\alpha^{(n)} L_0} \theta_0^2 + O(\theta_0^4).$$

As a consequence, $s_0^{(n)}$ must be small compared to $S_0^{(n,s)}$ (which is by construction limited to the range $0 \leq S_0^{(n,s)} \leq 1$). Thus a reasonable restriction is

$$|s_0^{(n)}| \lesssim 0.5. \qquad (45)$$

As shown in Fig. 10, evaluating this relation at the onset of the instability reduces significantly the physically reasonable range for some parameters. This restriction applies only for the nematic material parameters and, in general, nothing can be said about the corresponding smectic parameters. We will, however, take the smectic parameters in the same range as the nematic ones. If not indicated otherwise we used
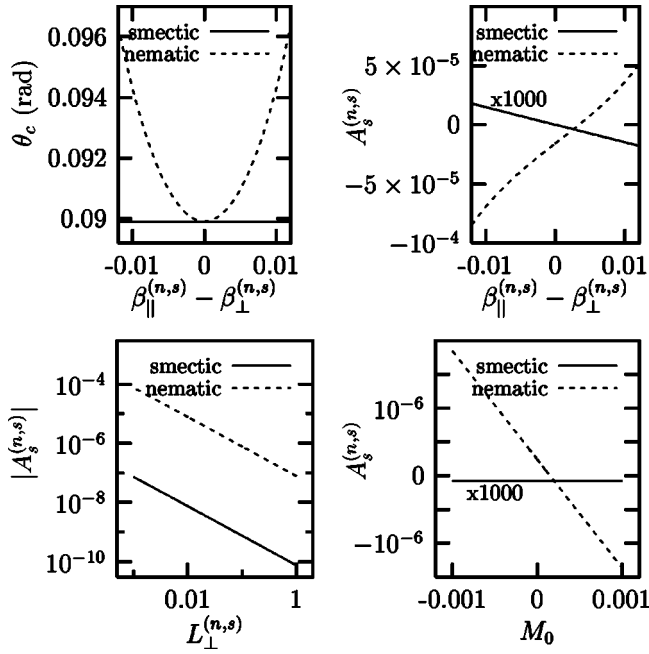
FIG. 11. Out of the material parameters connected with the order parameter, only $\beta_\parallel^{(n,s)} - \beta_\perp^{(n,s)}$ has a measurable effect on the critical values. Some more parameters can influence the amplitudes of the order parameter undulation, namely, $L_\perp^{(n,s)}$ and M_0 (the latter one is only present in the case of the nematic order parameter). All amplitudes have been normalized such that $A_\phi = 1$. Note that the smectic $A_s^{(s)}$ has been multiplied by 10^3 in the right column. For a better comparison we used a log-log scale in the lower left plot and changed the sign of $A_s^{(s)}$ in this plot.

$L_0^{(n,s)} = 0.1$, $\quad L_\perp^{(n,s)} = 0.01$, $\quad L_\parallel^{(n,s)} - L_\perp^{(n,s)} = 0.005$, $\quad M_0 = 10^{-4}$, $\quad \beta_\perp^{(n,s)} = 0.01$, $\quad \beta_\parallel^{(n,s)} - \beta_\perp^{(n,s)} = 0.005$, $\quad \alpha^{(n,s)} = 0.001$ for the plots of this section (along with parameter set specified in the preceding section).

The ansatz for $s_1^{(n,s)}$ following Eq. (35) reads

$$s_1^{(n,s)} = A_s^{(n,s)} \exp\left[\left(i\omega + \frac{1}{\tau}\right)t\right]\sin(q_z z)\cos(q y). \quad (46)$$

The modulations of $S^{(n,s)}$ in the linear analysis are maximum at the boundaries and in phase with the layer displacement u. The sign of the amplitude $A_s^{(n,s)}$ depends on the coupling to the velocity field (only the anisotropic part $\beta_\parallel^{(n)} - \beta_\perp^{(n)}$ is relevant) and on the coupling to the director undulations (via M_{ijk}, only for the nematic amplitudes $A_s^{(n)}$). If one assumes that shear reduces (and does not increase) the modulus of the order parameter, the nematic $\beta_\parallel^{(n)} - \beta_\perp^{(n)}$ is positive [Eqs. (39) and (41)]; once again nothing can be said about the smectic $\beta_\parallel^{(s)} - \beta_\perp^{(s)}$.

In general, the critical values are not at all or only very slightly influenced by the coupling to the modulus of the order parameter (see Fig. 11). Figure 11 summarizes the parameters with the largest influence on $A_s^{(n,s)}$. In almost all investigated cases the modulation of the nematic order is much larger than in the smectic order. Whether the order is reduced or increased in regions where the layers are com-

pressed depends in the phenomenological constants $\beta_\parallel^{(n,s)} - \beta_\perp^{(n,s)}$ and M_0, which have not been measured up to now.

The above results reveal some interesting features. As shown in Table III, the modulations of the order parameter change sign under inversion of the z axis. Considering the boundary condition (i.e., taking our ansatz), this leads to the fact that the effect on the modulus of the order parameters is maximum at the boundaries. So the linear analysis predicts that the regions where the order parameter is influenced most by the undulations are close to the boundaries. Since the probability for the formation of defects is higher in places where the order parameter is lower, we have identified areas where the creation of defects is facilitated. But our analysis does not allow to predict the structure of the defects. Nevertheless, this effect gives a possible way to reorient the parallel layers. Interestingly, experiments in block copolymers by Laurer *et al.* [3] show a defect structure close to the boundaries, which is consistent with this picture.

C. Oscillatory instability

All our arguments in the previous sections were based on the assumption that the undulations set in as a stationary instability. That is, that the oscillation rate ω in our ansatz Eq. (35) vanishes at onset. In this section we will discuss the situation for nonzero ω and find that our previous assumption was justified. In our linear analysis enters now (for the first time in this paper) the mass density of the system, which we will choose to be equal to unity, $\rho = 1$.

The search for a possible oscillatory instability is slightly different from the procedure used in the stationary case. The solvability condition of the linearized set of equations determines both the neutral curve and the frequency along this curve. When searching for such a solution we scanned approximately the same parameter space as used for Figs. 5–7. Since the frequency tends to zero when the oscillatory neutral curve gets close to the stationary one, we concentrated on the frequency range $0 \leq \omega \leq 2$ and check in some cases for higher frequencies.

It turned out that only in cases when the director field is very weakly coupled to the layering a neutral curve for an oscillatory instability is possible. This weak coupling manifests itself in small B_1 and γ_1, which is, in our set of dimensionless variables, equivalent to large B_0 and ν_i. Oscillatory neutral curves were only found for $B_0 \gtrsim 100$ or $\nu_i \gtrsim 1$. In all investigated cases a oscillatory neutral curve is either absent or lies above the neutral curve for a stationary instability. When an oscillatory neutral curve is possible, it ends in the points where it meets the stationary neutral curve (see Fig. 12). The corresponding frequency approaches zero in the end points of the oscillatory neutral curve. If we ignore for the moment the stationary neutral curve and consider only the oscillatory instability, the corresponding critical values are found to be rather close to the stationary one and to approach them the weaker the coupling between the director and the layers becomes. To summarize, an oscillatory instability was not found to be possible in all investigated cases and seems to be extremely unlikely to occur.
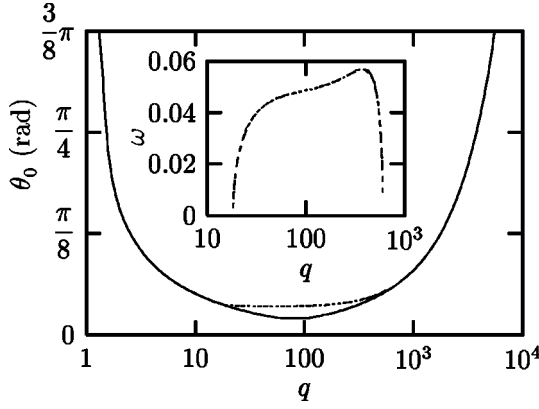
FIG. 12. In most parts of the scanned parameter space, no possibility for an oscillatory instability was found. If the director field is only very weakly coupled to the layering (in this plot we used $B_0 = 50$ and $\nu_i = 5$) a neutral curve for an oscillatory instability $(- - -)$ appears above the stationary neutral curve (——). Note that the critical wave vectors are close to each other for both oscillatory and stationary instability. The inset shows the frequency along the neutral curve.

D. Anisotropic viscosity

In Fig. 8 we have illustrated that a small viscosity coefficient ν_2 facilitates the onset of undulations. In this section we will have a closer look at the effect of an anisotropic viscosity tensor and ask whether undulations can be caused only due to viscosity effects without any coupling to the director field (i.e., we consider standard smectic-A hydrodynamics in this section).

Let us start our considerations by looking at the spatially homogeneous state. In a sample with parallel alignment the apparent viscosity is ν_3, which can easily be seen from the force on the upper boundary,

$$\vec{F}_{\parallel} = \hat{e}_z \underline{\sigma} = \dot{\gamma} \nu_3 \hat{e}_x. \tag{47}$$

Similarly, the viscosity of a perpendicular alignment is given by ν_2,

$$\vec{F}_{\perp} = \hat{e}_z \underline{\sigma} = \dot{\gamma} \nu_2 \hat{e}_x. \tag{48}$$

For $\nu_2 < \nu_3$ a simple shear flow in a perpendicular alignment causes less dissipation than in a parallel alignment. The next step is to study the stability of these alignments in the linear regime. Following the standard procedure (as described above) we find a solvability condition of the linearized equations which does not depend on the shear rate $\dot{\gamma}$,

$$0 = \{q^2 + \lambda_p [\nu_3 (q^2 - q_z^2)^2 + 2(\nu_2 + \nu_3) q^2 q_z^2]\} (B_0 q_z^2 + K q^4)$$
$$\times (\nu_2 q^2 + \nu_3 q_z^2). \tag{49}$$

Consequently, a parallel alignment of smectic layers is linearly stable against undulations even if the perpendicular alignment might be more preferable due to some thermodynamic considerations. As we have shown in Fig. 8, this rigorous result of standard smectic-A hydrodynamics is weakened in our extended formulation of smectic-A

hydrodynamics. When the director can show independent dynamics, an appropriate anisotropy of the viscosity tensor can indeed reduce the threshold values of an undulation instability.

IV. COMPARISON TO EXPERIMENTS AND SIMULATIONS

In the previous sections we have shown that the inclusion of the director of the underlying nematic oder in the description of a smectic-A-like system leads to some important features. In general, the behavior of the director under external fields differs from the behavior of the layer normal. In this paper we only discussed the effect of a velocity gradient, but the effects presented here seem to be of a more general nature and can also be applied to other fields. The key results of our theoretical treatment are a tilt of the director, which is proportional to the shear rate, and an undulation instability which sets in above a threshold value of the tilt angle (or equivalently the shear rate).

Both predictions are in agreement with experimental observations. For side-chain liquid crystalline polymers Noirez [15] observed a shear dependence of the layer thickness. In the parallel orientation the layer thickness is reduced by several percent with increasing shear. To our knowledge, two groups have investigated the evolution of a parallel alignment to the vesicle state for lyotropic systems (see Müller et al. [11] and Zipfel et al. [41]). In both papers the authors argue that cylindrical structures (with an axis along the flow direction) are observable as intermediates. These observed cylindrical intermediates are very close to the undulations proposed by our theoretical treatment.

For an approximate quantitative comparison of our theoretical results with the experiments on lyotropic liquid crystals we make a number of assumptions about the material parameters. As we have shown in Sec. III B, the different approaches cause only small variations in the critical wave number. For this estimate it suffices to use the critical wave number obtained in our earlier work [see Eq. (A2)]. For lyotropic liquid crystals it is known [42,43] that the elastic constants can be expressed as

$$K = \frac{\kappa}{l} \tag{50}$$

and

$$B = \frac{9}{64} \pi^2 \frac{(k_B T)^2}{\kappa} \frac{l}{(l - \delta)^4}, \tag{51}$$

where $\kappa = \alpha_\kappa k_B T$ is the bending modulus of a single bilayer, l is the repeat distance, δ is the membrane thickness, k_B is the Boltzmann constant, T is temperature, and α_κ is a dimensionless number of order of unity. With these relations we can estimate the critical wave vector for a sample of thickness d using Eq. (A2),

$$q_c^2 \approx \frac{3 \pi^2}{8 \alpha_\kappa d} \frac{l}{(l - \delta)^2}. \tag{52}$$

The parameters of the experiment by Zipfel *et al.* [41] are: $d = 1$ mm, $\delta = 2.65$ nm, $l = 6.3$ nm, and $\alpha_\kappa = 1.8$ [41,44]. On this basis we estimate the critical wavelength to be of the order of

$$\lambda_c \approx 6.4 \quad \mu\text{m}. \tag{53}$$

Zipfel *et al.* [41] observed a vesicle radius of 3 μm, which is clearly compatible with our calculation. We note that this estimate assumes that the experiments are done in the hydrodynamic regime.

In Sec. III B 3 we have pointed out that the effect on the order parameter is maximum close to the boundaries of the layer. In a reoriented sample Laurer *et al.* [3] have identified defects near the boundary of the sample which are in accordance with the predicted influence on the order parameter.

Molecular dynamic simulations recently made by Soddemann *et al.* [45] offer a very precise insight into the behavior of the layered systems under shear. Direct comparison of these simulations to the analytic theory presented above show a very good agreement between both approaches [40].

The mechanism we have proposed here is somewhat similar to a shear induced smectic-*C*-like situation. Consequently, undulations should also be observed near the smectic-*A*–smectic-*C* transitions. Indeed, Johnson and Saupe [46], and later Kumar [47], reported such undulations just below the transition temperature. In the same spirit, Ribotta and Durand [48] reported a compression induced smectic-*C*-like situation.

To conclude, we have shown in this work that the inclusion of nematic degrees of freedom in the description of smectic-*A*-like systems opens the way for a shear induced destabilization of the layers under shear. Our result are compatible with experimental observations and are in good agreement with molecular dynamics simulations.

APPENDIX A: MINIMAL ANALYTIC MODEL

In our earlier work [25] we considered two independent variables (the layer displacement and the *y* component of the director) and found the critical values to be

$$n_{x,c}^2 = 4 \frac{B_0}{B_0 - 2B_1} q_z \sqrt{\frac{K}{B_0}} \tag{A1}$$

and

$$q_c^2 = q_z \sqrt{\frac{B_0}{K}}. \tag{A2}$$

To compare our present analysis to these results we expand Eqs. (43) and (44) in power series in θ_0 (up to θ_0^2) and take only the terms connected with ϕ and u,

$$0 = A_\phi \frac{B_1}{\gamma_1} \theta_0 - A_u \frac{B_1}{\gamma_1} q, \tag{A3}$$

$$0 = -A_u \lambda_p \left[B_1 q^2 + K q^4 + B_0 q_z^2 - \frac{1}{2} \theta_0^2 q^2 (B_0 + 2B_1) \right] + A_\phi \lambda_p B_1 \theta_0 q. \tag{A4}$$

The solvability condition of Eqs. (A3) and (A4) defines the neutral curve $\theta_0(q)$ and its minimum directly gives the critical values θ_c and q_c (within the approximations of this section),

$$q_c^2 = q_z \sqrt{\frac{B_0}{K}}, \tag{A5}$$

$$\theta_c^2 = 4 q_z \frac{B_0}{B_0 + 2B_1} \sqrt{\frac{K}{B_0}}, \tag{A6}$$

$$\dot{\gamma}_c = 4 \frac{B_1}{\gamma_1(\lambda + 1)} \sqrt{q_z \frac{B_0}{B_0 + 2B_1} \sqrt{\frac{K}{B_0}}}. \tag{A7}$$

The differences between Eqs. (A1) and (A2), and (A5)–(A7) are mainly due to the correct normalization of $\hat{p}$ [see Eqs. (29)–(31)] used in the present paper.

To summarize, we conclude that our former results are a special case of the present analysis when the correct normalization of $\hat{p}$ is implemented. Especially, the divergence of the critical values at $B_0 = 2B_1$ turns out to be an artifact of the normalization of $\hat{p}$ used in Ref. [25].

APPENDIX B: GENERATING THE SET OF LINEAR EQUATIONS

Since the theoretical methods used in this paper (irreversible thermodynamics and linear stability analysis) offer well defined algorithms for the generation and analysis of macroscopic hydrodynamic equations, we performed parts of the calculation using Maple. In this appendix we describe the key ingredients of a suitable Maple program. A good starting point for such an approach are the balance equations for the unknown quantities (16), (18)–(20), (27), and (28) along with the energy density (1) in the appropriate approximation. These equations are entered directly in Maple, with the unknown quantities being functions of time and the spatial coordinates. The thermodynamic forces used in these equations are determined by Eqs. (13)–(14). For an implementation of these equations one must take into account that Maple can only compute the derivative with respect to constants and not with respect to functions, i.e., the relevant functions in the energy density must be substituted temporarily by constants.

For the linearized set of equations we substitute the unknown quantities by expressions of the type

$$\theta(t,x,y,z) = \theta_0 + a A_\theta \sin(q_z z) \cos(qy) \exp(i\omega t) \tag{B1}$$

in the governing equations. Here *a* is a small parameter and A_θ is the relative amplitude of the linear correction to θ_0. Expanding the substituted set of equations in a power series

in a gives in zeroth order the spatially homogeneous equations and in first order the linear set of equations, which are no longer differential equations but algebraic ones. One obtains a matrix representation of these equations by expanding them in power series of the relative amplitudes and taking only the first order terms. After dividing by the terms which depend on the spatial and temporal coordinates the FORTRAN code of this matrix representation is generated using the CODEGEN, FORTRAN function of Maple and subsequently solved using standard numerical procedures.

[1] V. K. Gupta, R. Krishnamoorti, Z.-R. Chen, J. A. Kornfield, S. D. Smith, M. Satkowski, and J. T. Grothaus, Macromolecules **29**, 875 (1996).

[2] U. Wiesner, Macromol. Chem. Phys. **198**, 3319 (1997).

[3] J. H. Laurer, B. Scott Pinheiro, D. L. Polis, and K. I. Winey, Macromolecules **32**, 4999 (1999).

[4] J. L. Zryd and W. R. Burghardt, Macromolecules **31**, 3656 (1998).

[5] H. Leist, D. Maring, T. Thurn-Albrecht, and U. Wiesner, J. Chem. Phys. **110**, 8225 (1999).

[6] D. L. Polis, S. Smith, N. J. Terrill, A. J. Ryan, D. C. Morse, and K. I. Winey, Macromolecules **32**, 4668 (1999).

[7] R. G. Horn and M. Kléman, Ann. Phys. (France) **3**, 229 (1978).

[8] C. R. Safinya, E. B. Sirota, and R. J. Plano, Phys. Rev. Lett. **66**, 1986 (1991).

[9] P. Panizza, P. Archambault, and D. Roux, J. Phys. II **5**, 303 (1995).

[10] O. Diat, D. Roux, and F. Nallet, J. Phys. II **3**, 1427 (1993).

[11] S. Müller, C. Börschig, W. Gronski, C. Schmidt, and D. Roux, Langmuir **15**, 7558 (1999).

[12] J. I. Escalante and H. Hoffmann, Rheol. Acta **39**, 209 (2000).

[13] J. Zipfel, P. Lindner, M. Tsianou, P. Alexandridis, and W. Richtering, Langmuir **15**, 2599 (1999).

[14] L. Noirez and A. Lapp, Phys. Rev. Lett. **78**, 70 (1997).

[15] L. Noirez, Phys. Rev. Lett. **84**, 2164 (2000).

[16] H. Wang, M. C. Newstein, A. Krishnan, N. P. Balsara, B. A. Garetz, B. Hammouda, and R. Krishnamoorti, Macromolecules **32**, 3695 (1999).

[17] P. G. de Gennes, Solid State Commun. **10**, 753 (1972).

[18] P. C. Martin, O. Parodi, and P. S. Pershan, Phys. Rev. A **6**, 2401 (1972).

[19] P. G. de Gennes and J. Prost, *The Physics of Liquid Crystals* (Clarendon Press, Oxford, 1993).

[20] H. Pleiner and H. R. Brand, *Pattern Formation in Liquid Crystals* (Springer, New York, 1996), Chap. 2.

[21] M. Delaye, R. Ribotta, and G. Durand, Phys. Lett. **44A**, 139 (1973).

[22] N. A. Clark and R. B. Meyer, Appl. Phys. Lett. **22**, 493 (1973).

[23] P. Oswald and S. I. Ben-Abraham, J. Phys. (France) **43**, 1193 (1982).

[24] A. S. Wunenburger, A. Colin, T. Colin, and D. Roux, Eur. Phys. J. E **2**, 277 (2000).

[25] G. K. Auernhammer, H. R. Brand, and H. Pleiner, Rheol. Acta **39**, 215 (2000).

[26] G. K. Auernhammer, H. R. Brand, and H. Pleiner, Proceedings Freiburger Arbeitstagung Flüssigkristalle **29**, V19 (2000).

[27] R. Bruinsma and Y. Rabin, Phys. Rev. A **45**, 994 (1992).

[28] A. G. Zilman and R. Granek, Eur. Phys. J. B **11**, 593 (1999).

[29] D. R. M. Williams and F. C. MacKintosh, Macromolecules **27**, 7677 (1994).

[30] P. G. de Gennes, Mol. Cryst. Liq. Cryst. **21**, 49 (1973).

[31] J. D. Litster, J. Als-Nielson, R. J. Birgeneau, S. S. Dana, D. Davidov, F. Garcia-Golding, M. Kaplan, C. R. Safinya, and R. Schaetzing, J. Phys. Colloq. **40**, C3 (1979).

[32] S. Garoff and R. B. Meyer, Phys. Rev. Lett. **38**, 848 (1977).

[33] S. R. de Groot and P. Mazur, *Non-Equilibrium Thermodynamics* (North-Holland, Amsterdam, 1962).

[34] M. Liu, Phys. Rev. A **19**, 2090 (1979).

[35] H. R. Brand and K. Kawasaki, J. Phys. C **19**, 937 (1986).

[36] J. Marignan, O. Parodi, and E. Dubois-Violette, J. Phys. (France) **44**, 263 (1983).

[37] H. Pleiner and H. R. Brand, Physica A **265**, 62 (1999).

[38] D. Forster, T. C. Lubensky, P. C. Martin, J. Swift, and P. S. Pershan, Phys. Rev. Lett. **26**, 1016 (1971).

[39] H.-H. Graf, H. Kneppe, and F. Schneider, Mol. Phys. **77**, 521 (1992).

[40] T. Soddemann, G. K. Auernhammer, H. X. Guo, B. Dünweg, and K. Kremer (to be published).

[41] J. Zipfel, F. Nettesheim, P. Linder, T. D. Le, U. Olsson, and W. Richtering, Europhys. Lett. **53**, 335 (2001).

[42] W. Helfrich, Z. Naturforsch. A **33A**, 305 (1978).

[43] F. Nallet, D. Roux, and J. Prost, J. Phys. (France) **50**, 3147 (1989).

[44] H. von Berlepsch and R. de Vries, Eur. Phys. J. E **1**, 141 (2000).

[45] T. Soddemann, B. Dünweg, and K. Kremer, Eur. Phys. J. E **6**, 409 (2001).

[46] D. Johnson and A. Saupe, Phys. Rev. A **15**, 2079 (1977).

[47] S. Kumar, Phys. Rev. A **23**, 3207 (1981).

[48] R. Ribotta and G. Durand, J. Phys. (France) **38**, 179 (1977).